Assessing Finite-Control-Set Model Predictive Control

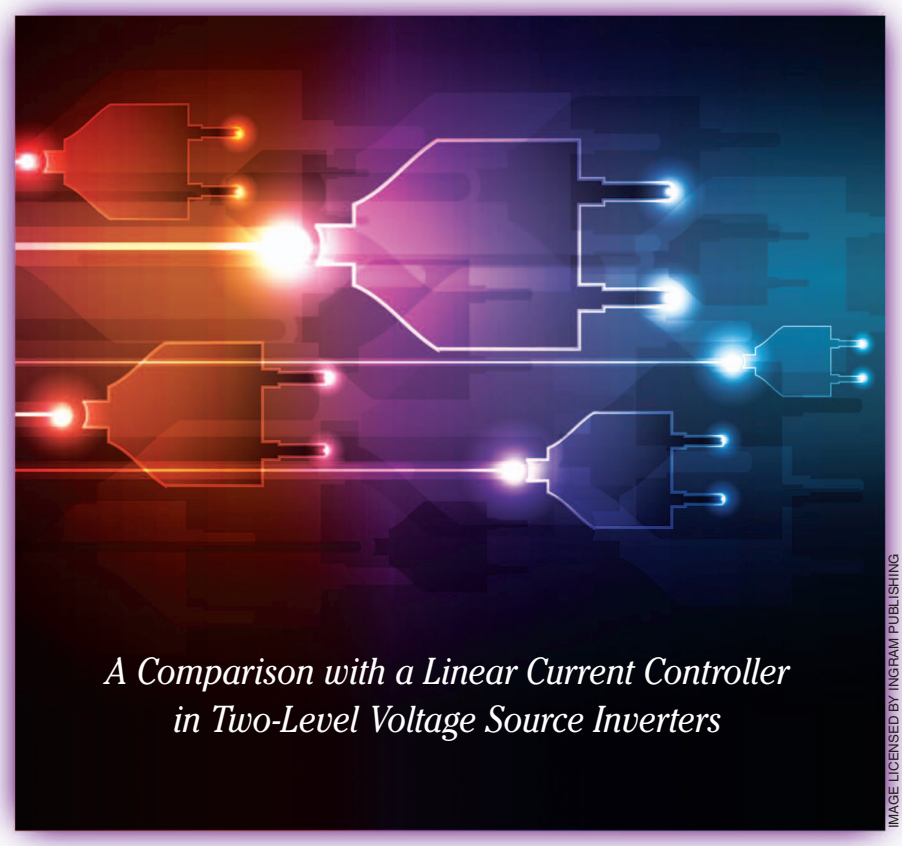

IMAGE LICENSED BY INGRAM PUBLISHING

HECTOR A. YOUNG,
MARCELO A. PEREZ,
JOSE RODRIGUEZ,
and HAITHAM ABU-RUB

Digital Object Identifier 10.1109/MIE.2013.2294870
Date of publication: 19 March 2014

Model predictive control (MPC) methods for applications in power converters have received considerable attention in recent years. The idea behind MPC is to use a mathematical model of the system to predict its future behavior within a predefined time. An optimization problem that includes the control objectives, the predicted variables, and possible constraints of the system is solved, yielding the control actions to be applied.

This technique can be divided in two wide categories: continuous-control-set MPC (CCS-MPC) and finite-control-set MPC (FCS-MPC) [1], [2]. The main differences are the way the optimization is performed and how the control actions are applied. With CCS-MPC schemes, the controller output is a continuous reference signal, which is converted to a suitable control action using a modulator. On the other hand, FCS-MPC takes advantage of the limited number of switching states available in the power converters for solving the optimization problem using a simple iterative algorithm. Once the optimal switching state is found, it is directly

1932-4529/14/$31.00©2014IEEE

applied to the converter and remains fixed during each switching period.

The FCS-MPC technique has several advantages that make it attractive for the control of power converters: its ease of implementation, particularly for one-step prediction horizons; its flexibility in the definition of control objectives; and its fast dynamic response [3]. Applications of FCS-MPC with extended prediction horizons have been presented for the simultaneous control of several objectives, such as torque, stator flux, and inverter neutral point potential, also including restrictions for the switching frequency [4]. However, because of the simplicity of its implementation, FCS-MPC schemes with one-step prediction horizons have received considerable attention in the last several years [5]. Despite the promising results of the FCS-MPC applications, some drawbacks have also been reported, such as variable switching frequency, which may cause greater switching losses and unwanted resonances [1], [6]. Another relevant problem is the nonzero steady-state error (SSE) in the FCS-MPC, especially when operating with lower switching frequencies or small current reference amplitudes [7], [8].

To obtain an insight into the abilities of the FCS-MPC for controlling power converters, it is necessary to carry out a comparison of its performance versus that of already established methods. Some of the works presenting applications of FCS-MPC have made performance comparisons versus linear controllers based on pulse-width modulation (PWM) [9], [10]. However, their comparison results mainly consist of qualitative analyses of factors such as waveforms and current and voltage spectra in a single operating point. A comparison between several MPC schemes and techniques based on PWM, space-vector modulation (SVM), and optimized pulse patterns for the control of a medium-voltage drive has been recently published [11]. That study considered as performance indices the current and torque distortion in function of the normalized switching losses. Although the comparison results were conclusive, aspects such as the transient behavior of the controllers and the SSE of the FCS-MPC were not addressed.

Another key aspect for the comparison between two control schemes is the switching frequency. Since FCS-MPC produces a variable switching frequency, in previous studies, the controller parameters and the operating point were adjusted to keep an average switching frequency similar to that of the PWM-based controllers used for comparison [12], [13]. Although this helps make a fair comparison of both control schemes, keeping a single operating point may hide interesting details about the behavior of the controllers in the whole operating range of the converter.

This article's objective is to experimentally compare the performance of FCS-MPC and a proportional integral (PI) controller in the synchronous dq frame with SVM (PI-SVM), both applied to the current control in a two-level voltage–source inverter (VSI). The comparison addresses the steady-state and dynamic response of the controllers by means of quantitative indices. Current-control schemes similar to the one considered here are key for applications where fundamental positive-sequence currents need to be controlled, such as in field-oriented control of electrical machines or real-reactive power controllers. Therefore, the results presented in this article may be helpful for evaluating the feasibility of FCS-MPC in such applications.

A resistive–inductive (RL) load in series with a voltage source is a common configuration in power electronics applications, where the voltage acts as a disturbance for the current-control system. However, in the present work, only the RL part of the load has been considered. This allows the attention to be focused on the tracking performance and steady-state behavior of the controllers rather than on complexities of the load or the rejection of external disturbances. The inclusion of a voltage source in the load will be considered in future works.

The FCS-MPC assessed in this work includes only the current tracking in the cost function, with a one-step prediction horizon. This basic implementation of the FCS-MPC has been selected because it makes it possible to carry out a more direct and fair comparison against the standard and well-accepted linear control methods. The comparison is carried out at different points throughout the operating range of the power converter, limited by the linear range attainable with SVM.

Current-Control Methods

The current controllers compared in this study are very different in nature. The PI-SVM computes continuous voltage references in base of the instantaneous control error and its integral. FCS-MPC, on the other hand, determines a set of switching signals for the power converter based on the future control error, which is predicted using a system model. The predictive method does not depend on the past values of the control error, as it is the case of PI-SVM, which has an integral component in its control law. This makes the transient response of the predictive controller faster, but at the price of lacking the ability to eliminate the SSE, which is an intrinsic characteristic of PI-SVM.

Another relevant feature of FCS-MPC is its independence from a modulation stage. This allows very fast dynamic responses to be obtained, since there is no delay associated with the modulation. Besides, the applied voltages to the load make always use of the full capacity of the inverter. This is not the case of controllers that depend on SVM, which, in general, are constrained to operate in the linear modulation range.

Synchronous PI Controller with SVM

PI current control in stationary $\alpha\beta$ coordinates presents nonzero SSE because of the lack of an integral component at frequencies different from zero [14]. For this reason, the PI control in rotating synchronous dq coordinates is often preferred [15]. In the recent literature, several enhancements for synchronous PI controllers can be found, such as time-delay compensation schemes [16], [17], complex-vector implementations [18], [19], or multivariable decoupling techniques [20], just to cite a few. Nevertheless, in this study,

we focus on the classic and conventional implementation of a PI controller with SVM to establish a comparison reference for the FCS-MPC.

Figure 1 shows the block diagram of the PI controller, which considers feed-forward terms for the decoupling of the d and q components of the current. For the modulation stage, an SVM has been implemented [21]. The coordinate rotations are made using the angle of the current reference θ^*.

Since the transient response of the linear controller depends strongly on the tuning of its parameters, for an unbiased comparison with the FCS-MPC, the design procedure of the PI controller is a relevant issue. In this work, the design method used is the magnitude optimum (MO) [22], which aims for the best set-point tracking given the restrictions imposed by the dynamics and delays of the system. The delay in an SVM-based system with switching period T_{SVM} can be modeled as the sum of a modulation delay and a processing delay introduced by the digital implementation and is commonly approximated by $1.5\,T_{\text{SVM}}$ [16]. As for the dynamics of the load, they are determined by its resistance and inductance parameters. The ratio of the PI gains are chosen so that $K_p/K_i = L/R$ to achieve a cancellation between the zero of the controller and the dominant pole of the plant. This step is similar to other PI design procedures in recent literature [17], [19]. Then, considering the modeled delays of the system, the MO method consists in calculating the proportional gain K_p that maximizes the range at which the magnitude of the closed-loop frequency response is unitary.

For the implementation of the PI-SVM, the physical limitations of the manipulated variables, i.e., the output voltages of the inverter, need to be considered. This is accomplished by saturating the reference voltages, which are the outputs of the controllers, to a range that do not exceed the modulation capacity of the SVM. The inclusion of these saturations in the control loop can give rise to the windup phenomenon, due to the integral component of the controllers. Therefore, to improve the transient response, an antiwindup scheme [23] has been included.

Finite-Control-Set Model Predictive Control

The FCS-MPC approach uses a discrete-time model for predicting the load current at a future sample period for each of the available output voltage vectors that can be generated by the inverter. A cost function is used to evaluate the predictions and to select the optimum voltage vector to be applied. The design of the cost function is a very important stage in the design of the FCS-MPC, since it contains the control objectives and also any constraints that need to be included.

The current control by means of FCS-MPC is usually implemented in stationary $\alpha\beta$ coordinates [3], [24]. Since the current references are sinusoidal, an extrapolation method, such as Lagrange polynomials, needs to be used to accurately predict the future current errors [9]. However, as the extrapolation is made taking into account past values of the reference, in the presence of a step change, the extrapolated reference exhibits unwanted oscillations, which have a negative influence in the transient response of the controller. To avoid this issue, in this study, the FCS-MPC was implemented in a rotating dq frame, synchronous with the current reference. Since the current references are continuous in this frame, no extrapolation methods are required.

In this article, a current model in the synchronous dq frame with forward Euler discretization is used

$$i_d(k+1) = i_d(k)\left(1 - \frac{RT_s}{L}\right) + \frac{T_s}{L}\left(v_d(k) + \omega^* L i_q(k)\right), \tag{1}$$

$$i_q(k+1) = i_q(k)\left(1 - \frac{RT_s}{L}\right) + \frac{T_s}{L}\left(v_q(k) - \omega^* L i_d(k)\right), \tag{2}$$

where R and L are the load resistance and inductance, respectively; T_s is the sampling period; and ω^* is the angular frequency of the current reference. The voltages v_d and v_q used for the current prediction in (1) and (2) depend on the dc-link voltage V_{dc} according to the following equations:

$$\begin{bmatrix} v_d(k) \\ v_q(k) \end{bmatrix} = \begin{bmatrix} \cos\theta^* & \sin\theta^* \\ -\sin\theta^* & \cos\theta^* \end{bmatrix} \begin{bmatrix} v_\alpha(k) \\ v_\beta(k) \end{bmatrix}$$

$$\begin{bmatrix} v_\alpha(k) \\ v_\beta(k) \end{bmatrix} = \frac{2}{3} V_{\text{dc}} \begin{bmatrix} 1 & -\frac{1}{2} & -\frac{1}{2} \\ 0 & \frac{\sqrt{3}}{2} & -\frac{\sqrt{3}}{2} \end{bmatrix} \begin{bmatrix} S_a(k) \\ S_b(k) \\ S_c(k) \end{bmatrix},$$

where v_α and v_β are the output voltages of the inverter in stationary $\alpha\beta$ coordinates, and S_a, S_b, and S_c are the switching signals for each phase of the inverter. Since the inverter's dc-link is not ideal, there exists ripple in this voltage. Therefore, to obtain a more accurate prediction, V_{dc} is measured at each sampling instant.

The cost function selected here for the control of the d and q components of the load current is the following:

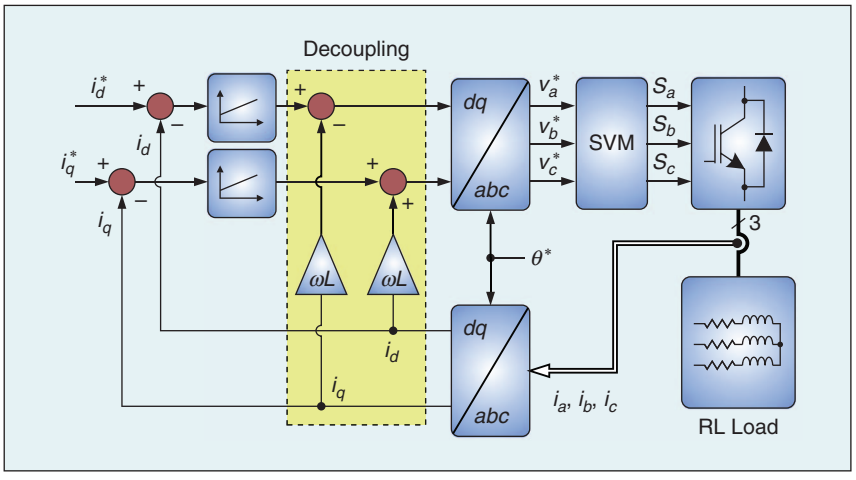

FIGURE 1 – A block diagram shows the synchronous PI controller with SVM.

$$g = |i_d^*(k+2) - i_d(k+2)| + |i_q^*(k+2) - i_q(k+2)|, \quad (5)$$

where the current predictions $i_d(k+2)$ and $i_q(k+2)$ are obtained by iterating (1) and (2), respectively. Here, the cost function is evaluated two time steps ahead to compensate for the computation delay in the digital implementation of the FCS-MPC algorithm [25].

A block diagram of the FCS-MPC is presented in Figure 2. The core of the predictive algorithm is the cost function minimization where, using the current references and predictions, the optimal switching signals are calculated and directly applied to the inverter. Since the FCS-MPC operates in the *dq* frame, coordinate rotations are required. Nonetheless, only one transformation is required instead of the two of them that are needed for the PI-SVM scheme.

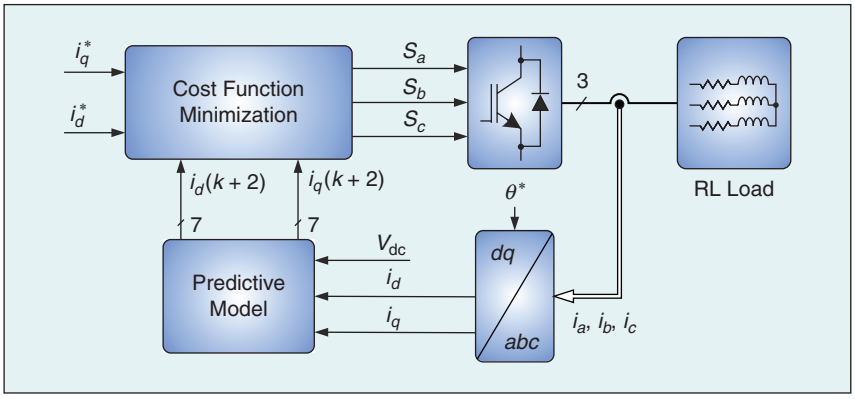

FIGURE 2 – A block diagram shows the FCS-MPC in the synchronous rotating *dq* frame.

Performance Indices

The main aspects of the controllers compared in this study have been presented in the preceding sections. It is clear that their working principles are quite different; however, they share the same control objective: to track the load current reference. The success in accomplishing this task can be measured in a number of ways; however, here, we focus on a few quantitative performance indices defined both for the steady-state and the transient response of the current controllers.

Steady-State Performance Indices

Weighted Total Harmonic Distortion

The total harmonic distortion (THD) is a well-known figure of merit for assessing the ability of a controller for tracking a sinusoidal reference. This index allows quantifying the proportion of harmonic components of a signal in respect of its fundamental component. Although the widespread use of THD as performance index, the weighted THD (WTHD) has been recognized as a more useful figure of merit, since it represents better the behavior of an inductive load [26]. The WTHD is defined as [27]

$$\text{WTHD} = \frac{\sqrt{\sum_{j\neq 1}\left(\frac{V_{j,\text{RMS}}}{j}\right)^2}}{V_{1,\text{RMS}}} \times 100, \quad (6)$$

where j is the harmonic index, $V_{j,\text{RMS}}$ is the root mean square (RMS) value of the jth harmonic component, and $V_{1,\text{RMS}}$ is the RMS value of the fundamental component of the load phase voltage, respectively.

Steady-State Error

The SSE is a very relevant aspect for the performance evaluation of a control scheme. In this work, the SSE is measured in the *dq* coordinate system. Considering a number N of current samples, the mean values of the control error for each axis, $\overline{\varepsilon_d}$ and $\overline{\varepsilon_q}$, are calculated as follows:

$$\overline{\varepsilon_d} = \frac{1}{N}\sum_j (i_d^*[j] - i_d[j]) \quad (7a)$$

$$\overline{\varepsilon_q} = \frac{1}{N}\sum_j (i_q^*[j] - i_q[j]), \quad (7b)$$

where i_d^*, i_q^* are the current references and i_d, i_q are the current measurements in the d and q axes, respectively. Consequently, the SSE is calculated by

$$\text{SSE} = \frac{\sqrt{\overline{\varepsilon_d}^2 + \overline{\varepsilon_q}^2}}{\sqrt{i_d^{*2} + i_q^{*2}}} \times 100. \quad (8)$$

Average Switching Frequency

The switching frequency and the power losses in the semiconductors of the converters are directly related. On the other hand, it is a key parameter that determines aspects such as the response time, bandwidth, and current harmonic distortion [21], [28]. This creates a fundamental tradeoff between power losses and control quality.

In PWM-based schemes, the switching frequency is constant. However, in the case of FCS-MPC, the average switching frequency is variable and depends mainly on the sampling period of the control algorithm, the load characteristics, and the operating point [6], [29]. Another aspect that influences the behavior of the average switching frequency of FCS-MPC schemes is the design of the cost function. Examples of this can be found in the work of Cortés et al. [30], where spectral shaping of the current was imposed, and in the work of Geyer [11], where the minimization of switching losses was considered. Although the aforementioned publications show that the average switching frequency can be manipulated in FCS-MPC schemes, in this article, we maintain the focus on the basic FCS-MPC to analyze the variability of the switching frequency and its impact on the performance of the current control.

To evaluate the average switching frequency of FCS-MPC, the following expression is used:

$$\overline{f_{\text{sw}}} = \frac{1}{3}\frac{N_a + N_b + N_c}{T}, \quad (9)$$

where N_a, N_b, and N_c are the number of switching cycles in one switch of the phases a, b, and c of the inverter, respectively; and T is the period considered for the calculation of the average switching

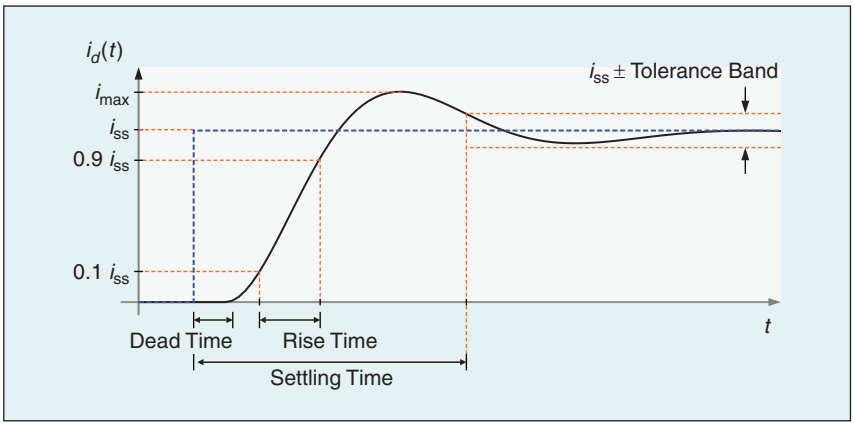

FIGURE 3 – The definition of the transient performance indices.

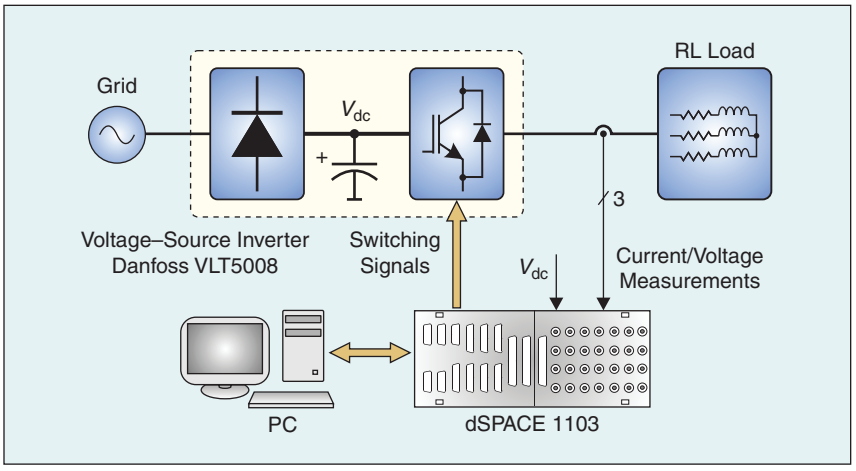

FIGURE 4 – The experimental setup.

frequency, which is an integer multiple of the current fundamental period.

Transient-State Performance Indices

In a current-control system, the following parameters of the dynamic response can be considered to assess the performance of the controllers [15]: settling time, rise time, dead time, and overshoot factor (OF). These indices are well known [31] and can be calculated directly from the time response of the controlled currents, as depicted in Figure 3 for a generic second-order system. The transient performance of the controllers is evaluated in the *dq* frame, because the constant current references make the analysis easier. The settling time is defined as the time required for the current to stay in a tolerance band of ±5% or ±10% around the reference; the rise time is defined as the time required for the current to increase from 10% to 90% of the reference step change; the dead time is measured as the time between the reference change and the response in the controlled current. For the calculation of the OF, the following formula was used:

$$\text{OF} = \frac{i_{\max} - i_{ss}}{i_{ss}} \times 100, \qquad (10)$$

where $i_{\max}$ is the maximum or peak value of the transient response of the current, and i_{ss} is the value of the current in steady state.

Results

Experimental Setup

Figure 4 shows a diagram of the experimental setup used for this study. The power stage consists of a two-level VSI (Danfoss VLT5008) with a dc-link voltage of $V_{dc} = 100$ V and a three-phase RL load. The dead time for the power semiconductors in the inverter is hardware-implemented and has a value of 2 [μs]. The processing platform used for the implementation of the control algorithms is a dSPACE1103, connected to a personal computer for programming and data logging. The SVM implemented for the PI controller has a switching period $T_{SVM} = 250$ [μs], which is equal to the sampling time of the discrete linear controllers, according to the synchronized sampling method [32]. The PWM is generated by the slave digital signal processor unit of the dSPACE1103, a TMS320F240 with 16 b and a resolution of 50 [ns].

For the FCS-MPC, a sampling time $T_s = 50$ [μs] is considered. This value has been selected to obtain an average switching frequency similar to that of the PI-SVM in some of the operating points considered throughout this study. This aspect is very important for a fair comparison between both control schemes. The sampling of the measured variables used for the analysis and comparison of the control methods was performed using the same sampling period as the FCS-MPC. The results in this section are presented for operating points defined by the peak current reference i^* in per-unit notation, referred to the nominal current i_{nom}. Current references with a frequency $f^* = 50$ [Hz] and amplitudes ranging between 0.05 and 0.85 per unit (p.u.) (0.275 and 4.675 [A]) have been

TABLE 1 – THE PARAMETERS USED FOR THE EXPERIMENTAL RESULTS.

PARAMETER	VALUE	DESCRIPTION
R	10 [Ω]	Load resistance
L	10 [mH]	Load inductance
T_s	50 [μs]	Sampling period for FCS-MPC
T_{SVM}	250 [μs]	Sampling period for PI-SVM
i_{nom}	5.5 [A]	Nominal load current
f^*	50 [Hz]	Current reference frequency

used. The parameters considered in the experiments are presented in Table 1.

Steady-State Performance Comparison

Figure 5(a) shows the output voltage WTHD as a function of the normalized current reference. In the case of the FCS-MPC, it is remarkable how the distortion changes depending on the operating point; for very small references, the WTHD with FCS-MPC is about 50% larger than with the PI-SVM. However, for reference amplitudes greater than 0.15 [p.u.], the current distortion generated by the FCS-MPC is very close to that of the linear controller. The SSE shown in Figure 5(b) presents a similar behavior. At the lowest evaluated operation point (0.05 [p.u]), the SSE of FCS-MPC can reach up to 25%. Nonetheless, with increasing amplitudes of the current reference the SSE rapidly decreases to levels comparable to the obtained with the PI-SVM.

The average switching frequency of the controllers in the operating range is presented in Figure 5(c), where FCS-MPC shows the characteristic bell-shaped curve reported in [6]. By observing the three plots of Figure 5, it is clear that the poor performance of FCS-MPC at low operating points comes along with the noticeable decrease of average switching frequency in that range. This tradeoff between switching frequency and steady-state performance is well known in power electronics [11]. However, it can also be noted in Figure 5 that for operating points above 0.25 [p.u.], the steady-state performance of FCS-MPC is comparable to that of the PI-SVM, even at points where the average switching frequency of the predictive controller is noticeably lower than with the linear one. This is the case of current references above 0.65 [p.u.], where the FCS-MPC can provide a steady-state performance very similar to that of the PI-SVM controller, while maintaining a lower average switching frequency and, therefore, lower switching losses.

It is important to mention that one of the most noticeable issues with FCS-MPC is the spread harmonic spectrum it introduces due to the optimal voltage selection. This can be undesirable in some applications and might impose the need to include filters for the output current, thus increasing the cost, weight, and volume of the application. To quantitatively assess the distortion, in this study, the WTHD has been selected as a suitable index, but since it concentrates all the harmonic behavior in a single figure, the presence of individual harmonics in the controlled current cannot be evaluated. For this purpose, Figure 6 presents the magnitude of some individual load current harmonics throughout the operating range of the inverter using each of the evaluated controllers. The selected harmonics correspond to the odd ones between the third and the 17th. With FCS-MPC, the magnitude of the harmonics at low operating points (<0.15 [p.u.]) is significantly higher than with PI-SVM. This is consistent with the poor performance of FCS-MPC in terms of WTHD in this operating range, as it was presented in Figure 5. Nonetheless, for higher operating points (>0.25 [p.u.]) the magnitude of the observed harmonics with FCS-MPC is comparable with the performance of PI-SVM. Moreover, some low-order harmonics, such as the third, fifth, and seventh, present lower amplitudes with FCS-MPC than with PI-SVM for current references greater than 0.25 [p.u.].

Transient Performance Comparison

The transient responses of the PI-SVM and the FCS-MPC in the d and q axes are presented in Figure 7(a) and (b), respectively. Two step changes in the current reference are applied; the first from 0.1 to 0.85 [p.u.] at instant $t = 0.06$ [s], and the second from 0.85 to 0.55 [p.u.] at instant $t = 0.075$ [s]. In the dynamic response, the FCS-MPC is slightly faster than the PI-SVM, as can be confirmed by the performance indices in Table 2. The dead time observed in the response of the PI-SVM is 400 [μs], and it approximately matches the delay introduced by the modulation and the digital implementation of the controller, which using the approximation of $1.5\,T_{SVM}$ yields 375 [μs]. A relevant difference in the dynamic behavior of the controllers is the decoupling capability between the d and q axes. In Figure 7(b), it can be observed that, with the PI-SVM, the current in the q axis is disturbed when the step changes in the d axis current reference are applied (at $t = 0.06$ [s] and $t = 0.075$ [s]). This coupling is not noticeable in the response of the FCS-MPC. The waveforms of the controlled current in *abc* coordinates for a single reference step change, from 0.1 to 0.85 [p.u.] at instant $t = 0.06$ [s] are presented in Figure 8(a) and (b), respectively. In this reference frame, the dead time in the response of the PI-SVM can be clearly noticed, as well as oscillations around the current references. These phenomena are not present in the response of the FCS-MPC.

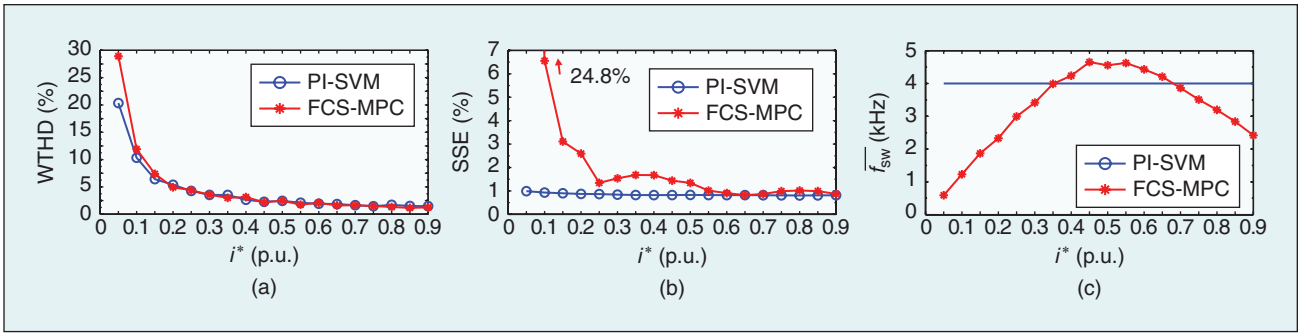

FIGURE 5 – (a) The output voltage WTHD, (b) load current SSE, and (c) average switching frequency are plotted as a function of the normalized current reference.

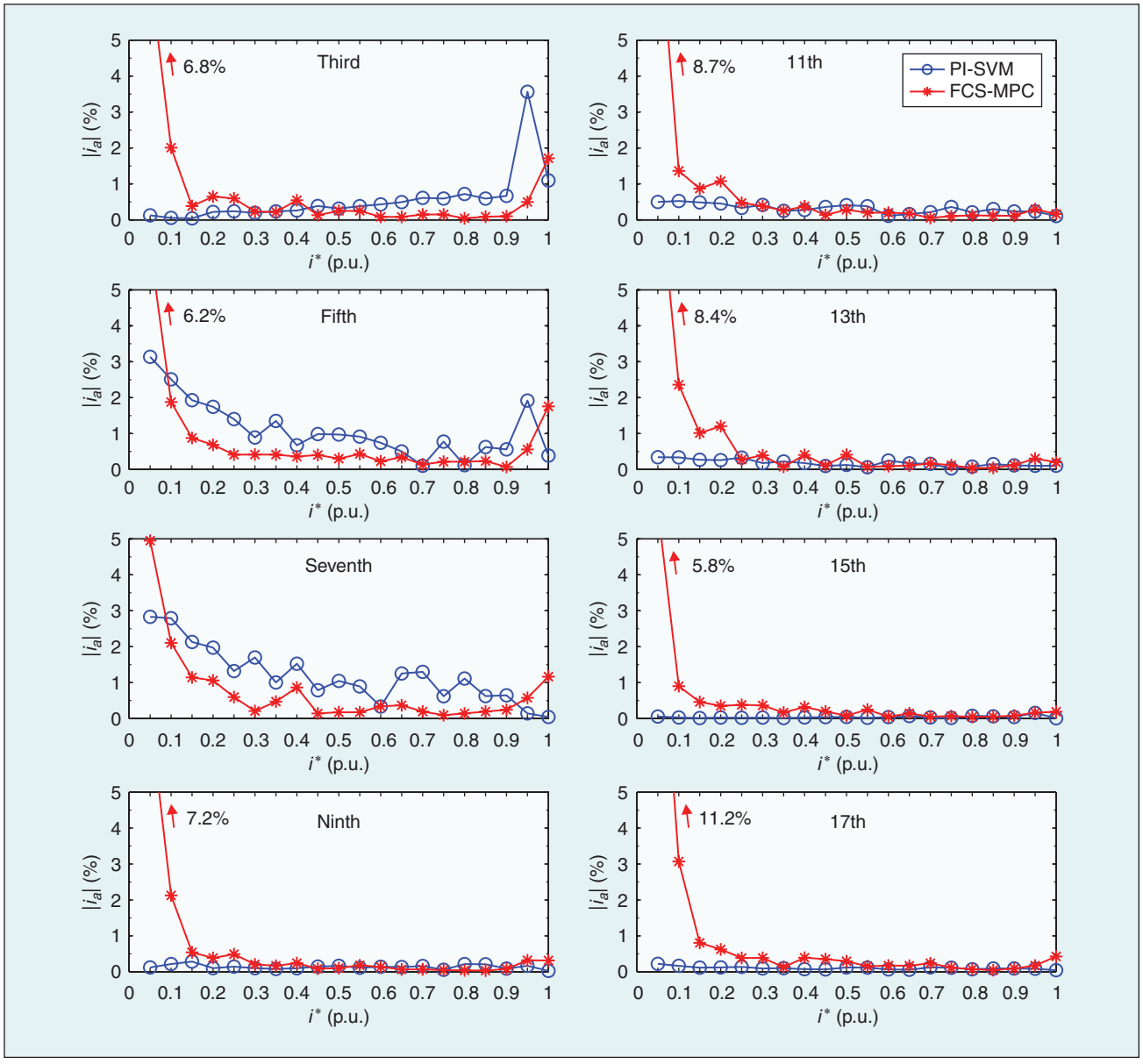

FIGURE 6 – The individual current harmonics plotted as a function of the normalized current reference.

Execution Times of the Control Algorithms

The execution times of the control algorithms in the dSPACE1103 control platform have been measured to assess the computing power requirement of the compared methods. Even though the FCS-MPC algorithm must estimate and predict the control actions for each of the available voltage vectors of the inverter at each sampling period, its execution time (4.9 [μs]) is not much greater than that of the PI-SVM (3.3 [μs]). This makes the FCS-MPC a feasible option for high-performance digital current-control applications such as field-oriented control.

TABLE 2 – THE TRANSIENT PERFORMANCE OF THE CONTROLLERS (*d* AXIS).

REFERENCE STEP	$i^* = 0.1 \rightarrow 0.85$ **(p.u.)**		$i^* = 0.85 \rightarrow 0.55$ **(p.u.)**	
	PI-SVM	FCS-MPC	PI-SVM	FCS-MPC
Rise time (ms)	1.49	1.40	1.02	0.13
Settling time (ms)[a]	6.71	1.92	1.45	0.18
Dead time (μs)	400	50	400	50
Overshoot (%)	7.48	–	8.49	–

[a]The settling times were calculated using a band of ±5% and ±10% for the reference steps to 0.85 [p.u.] and 0.55 [p.u.], respectively.

Conclusions

FCS-MPC is a new and conceptually different alternative to linear controllers with any kind of pulsewidth modulator. In this work, a comparative study between PI-SVM, a traditional linear controller, and FCS-MPC for the current

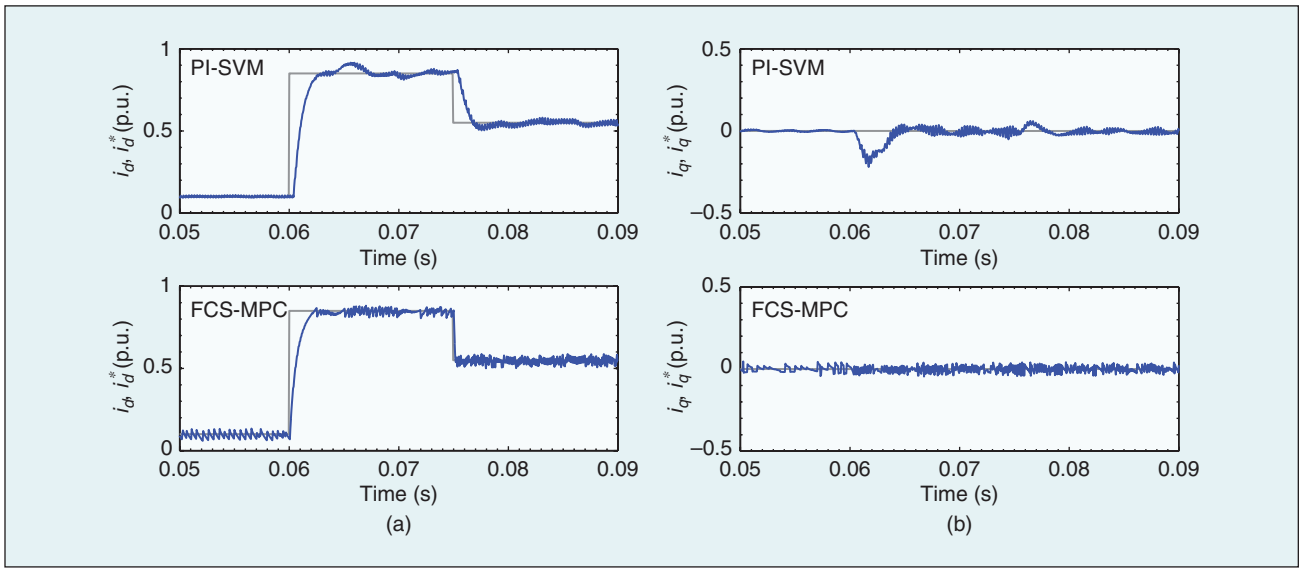

FIGURE 7 – The transient response in the synchronous *dq* frame: (a) *d* axis and (b) *q* axis.

control of a two-level VSI is presented. The well-known quantitative performance indices are used for assessing both the steady-state and transient behavior in several points throughout the inverter operation range.

The experimental results show that at low operating points the steady-state performance of FCS-MPC is poor in comparison with that of PI-SVM, presenting high current distortion and SSE. However, in most operating points the current distortion in terms of WTHD is very similar for both controllers. The study was complemented with the analysis of current spectra where, in the presence of harmonics in the dc-link voltage due to nonideal grid conditions, it was observed that FCS-MPC is able to generate waveforms with less low-order harmonics, such as third, fifth and seventh, than PI-SVM. The SSE of FCS-MPC is also comparable with that of PI-SVM in a wide range of operating points of the inverter, particularly with reference currents greater than 0.65 [p.u.]. At the same time, the average switching frequency of the FCS-MPC in this operating range is lower than that of the linear method. This implies that the FCS-MPC can provide an acceptable steady-state performance with lower switching losses than the PI controller.

Regarding the dynamic performance, the FCS-MPC shows a faster response than a conventional PI-SVM controller tuned by the MO method, also offering a better decoupling of the *d* and *q* components of the current. An additional advantage of the FCS-MPC is that it requires a much simpler implementation, since saturation of the manipulated variables, antiwindup protection, decoupling networks, and tuning of controller parameters are not required. The results presented in this article confirm that FCS-MPC is a competitive alternative to classical current-control methods.

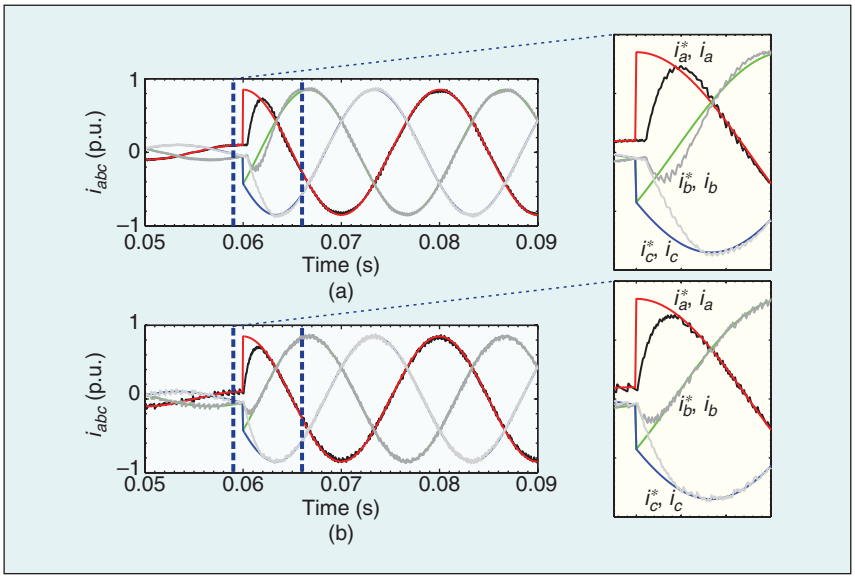

FIGURE 8 – The transient response in *abc* coordinates: (a) PI-SVM and (b) FCS-MPC.

Acknowledgments

This work was supported by the Chilean Comision Nacional de Investigacion Cientifica y Tecnologica (CONICYT) scholarship program for Ph.D. studies in Chile and the CONICYT Basal Funding Program FB0821. This publication was made possible by NPRP grant 4-077-2-028 from the Qatar National Research Fund (a member of the Qatar Foundation). The statements made herein are solely the responsibility of the authors.

Biographies

Hector A. Young (hector.young@postgrado.usm.cl) received his B.Eng. and M.Sc. degrees in electronics engineering in 2009 from the Universidad

de la Frontera, Temuco, Chile. He was granted a scholarship from the Chilean National Research, Science, and Technology Committee (CONICYT) in 2010 to pursue his Ph.D. studies in power electronics at the Universidad Técnica Federico Santa María, Valparaiso, Chile. His main research interest is model-based predictive control of power converters and drives. He is a Student Member of the IEEE.

Marcelo A. Perez received his engineering degree in electronic engineering, M.Sc. degree in electrical engineering, and D.Sc. degree in electrical engineering from the University of Concepcion, Chile, in 2000, 2003, and 2006, respectively. From 2006 to 2009, he held a postdoctoral position at the Universidad Tecnica Federico Santa Maria, Valparaiso, Chile, conducting research in the area of power converters. Since 2009, he has been an associate researcher there. His main interests are control of power converters, multilevel converters, and HVDC systems. He is a Member of the IEEE.

Jose Rodriguez received his engineering degree in electrical engineering from the Universidad Federico Santa Maria, Valparaiso, Chile, in 1977, and his Dr.-Ing. degree in electrical engineering from the University of Erlangen, Germany, in 1985. He has been with the Department of Electronics Engineering, University Federico Santa Maria, since 1977, where he is currently full professor and rector. He has coauthored more than 300 journal and conference papers. His main research interests include multilevel inverters, new converter topologies, control of power converters, and adjustable-speed drives. He has been an associate editor of *IEEE Transactions on Power Electronics* and *IEEE Transactions on Industrial Electronics* since 2002. He received the Best Paper Award from *IEEE Transactions on Industrial Electronics* in 2007, the Best Paper Award from *IEEE Industrial Electronics Magazine* in 2008, and the Best Paper Award from *IEEE Transactions on Power Electronics* in 2010. He is a member of the Chilean Academy of Engineering. He is a Fellow of the IEEE.

Haitham Abu-Rub received his Ph.D. degree from the Electrical Engineering Department, Technical University of Gdansk, Poland. He is currently a senior associate professor at Texas A&M University, Doha, Qatar. He has earned many prestigious international awards, including the American Fulbright Scholarship, the German Alexander von Humboldt Fellowship, the German DAAD Scholarship, and the British Royal Society Scholarship (at Southampton University). He has published more than 140 journal and conference papers. His main research focuses on electrical drive control, power electronics, and electrical machines. He is a Senior Member of the IEEE.

References

[1] P. Cortes, M. P. Kazmierkowski, R. M. Kennel, D. E. Quevedo, and J. Rodriguez, "Predictive control in power electronics and drives," *IEEE Trans. Ind. Electron.*, vol. 55, no. 12, pp. 4312–4324, 2008.

[2] A. Linder, R. Kanchan, R. Kennel, and P. Stolze, *Model-Based Predictive Control of Electric Drives*. Göttingen, Germany: Cuvillier Verlag, 2010.

[3] S. Kouro, P. Cortes, R. Vargas, U. Ammann, and J. Rodriguez, "Model predictive control—A simple and powerful method to control power converters," *IEEE Trans. Ind. Electron.*, vol. 56, no. 6, pp. 1826–1838, 2009.

[4] T. Geyer, G. Papafotiou, and M. Morari, "Model predictive direct torque control—Part I: Concept, algorithm, and analysis," *IEEE Trans. Ind. Electron.*, vol. 56, no. 6, pp. 1894–1905, 2009.

[5] J. Rodriguez, M. P. Kazmierkowski, J. R. Espinoza, P. Zanchetta, H. Abu-Rub, H. A. Young, and C. A. Rojas, "State of the art of finite control set model predictive control in power electronics," *IEEE Trans. Ind. Inform.*, vol. 9, no. 2, pp. 1003–1016, May 2013.

[6] U. Ammann, R. Vargas, and J. Roth-Stielow, "Investigation of the average switching frequency of direct model predictive control converters," in *Proc. 2010 IEEE Int. Conf. Industrial Technology*, pp. 1800–1807.

[7] P. Lezana, R. Aguilera, and D. Quevedo, "Steady-state issues with finite control set model predictive control," in *Proc. 35th Annu. Conf. IEEE Industrial Electronics, (IECON'09)*, 2009, pp. 1776–1781.

[8] R. P. Aguilera, P. Lezana, and D. E. Quevedo, "Finite-control-set model predictive control with improved steady-state performance," *IEEE Trans. Ind. Inform.*, vol. 9, no. 2, pp. 658–667, 2013.

[9] J. Rodriguez, J. Pontt, C. A. Silva, P. Correa, P. Lezana, P. Cortes, and U. Ammann, "Predictive current control of a voltage source inverter," *IEEE Trans. Ind. Electron.*, vol. 54, no. 1, pp. 495–503, 2007.

[10] F. Barrero, M. R. Arahal, R. Gregor, S. Toral, and M. J. Durán, "A proof of concept study of predictive current control for VSI-driven asymmetrical dual three-phase AC machines," *IEEE Trans. Ind. Electron.*, vol. 56, no. 6, pp. 1937–1954, 2009.

[11] T. Geyer, "A comparison of control and modulation schemes for medium-voltage drives: emerging predictive control concepts versus PWM-based schemes," *IEEE Trans. Ind. Applicat.*, vol. 47, no. 3, pp. 1380–1389, 2011.

[12] J. Rodriguez, R. Kennel, J. Espinoza, M. Trincado, C. Silva, and C. Rojas, "High performance control strategies for electrical drives: An experimental assessment," *IEEE Trans. Ind. Electron.*, vol. 59, no. 2, pp. 812–820, 2012.

[13] M. Rivera, A. Wilson, C. A. Rojas, J. Rodriguez, J. R. Espinoza, P. W. Wheeler, and L. Empringham, "A comparative assessment of model predictive current control and space vector modulation in a direct matrix converter," *IEEE Trans. Ind. Electron.*, vol. 60, no. 2, pp. 578–588, Feb. 2013.

[14] D. N. Zmood, S. Member, D. G. Holmes, and G. H. Bode, "Frequency-domain analysis of three-phase linear current regulators," *IEEE Trans. Ind. Applicat.*, vol. 37, no. 2, pp. 601–610, 2001.

[15] M. Kazmierkowski, R. Krishnan, and F. Blaabjerg, *Control in Power Electronics: Selected Problems*, 1st ed. New York: Academic, 2002.

[16] B.-H. Bae and S.-K. Sul, "A compensation method for time delay of full-digital synchronous frame current regulator of PWM AC drives," *IEEE Trans. Ind. Applicat.*, vol. 39, no. 3, pp. 802–810, May 2003.

[17] H. Kim, M. W. Degner, J. M. Guerrero, F. Briz, and R. D. Lorenz, "Discrete-time current regulator design for AC machine drives," *IEEE Trans. Ind. Applicat.*, vol. 46, no. 4, pp. 1425–1435, July 2010.

[18] F. Briz, M. Degner, and R. Lorenz, "Analysis and design of current regulators using complex vectors," *IEEE Trans. Ind. Applicat.*, vol. 36, no. 3, pp. 817–825, 2000.

[19] J. Holtz and N. Oikonomou, "Fast dynamic control of medium voltage drives operating at very low switching frequency–An overview," *IEEE Trans. Ind. Electron.*, vol. 55, no. 3, pp. 1005–1013, Mar. 2008.

[20] B. Bahrani, S. Kenzelmann, and A. Rufer, "Multivariable-PI-based dq current control of voltage source converters with superior axis decoupling capability," *IEEE Trans. Ind. Electron.*, vol. 58, no. 7, pp. 3016–3026, July 2011.

[21] B. Wu, *High Power Converters and AC Drives*, 1st ed. New York: Wiley-IEEE Press, 2006.

[22] K. Åström and T. Hägglund, *PID Controllers: Theory, Design, and Tuning*, 2nd ed. USA: The Instrumentation, Systems, and Automation Society (ISA), 1995.

[23] G. C. Goodwin, S. F. Graebe, and M. E. Salgado, *Control System Design*, 1st ed. Englewood Cliffs, NJ: Prentice Hall, 2000.

[24] S. Vazquez, J. I. Leon, L. G. Franquelo, J. M. Carrasco, E. Dominguez, P. Cortes, and J. Rodriguez, "Comparison Between FS-MPC Control Strategy for an UPS inverter application in $\alpha - \beta$ and abc frames," in *Proc. IEEE Int. Industrial Electronics (ISIE) Symp.*, 2010, pp. 3133–3138.

[25] P. Cortes, J. Rodriguez, C. Silva, and A. Flores, "Delay compensation in model predictive current control of a three-phase inverter," *IEEE Trans. Ind. Electron.*, vol. 59, no. 2, pp. 1323–1325, 2012.

[26] D. Holmes and T. Lipo, *Pulse Width Modulation for Power Converters: Principles and Practice*, 1st ed. New York: Wiley-IEEE Press, 2003.

[27] D. Holmes, "The significance of zero space vector placement for carrier-based PWM schemes," *IEEE Trans. Ind. Applicat.*, vol. 32, no. 5, pp. 1122–1129, 1996.

[28] M. H. Rashid, Ed., *Power Electronics Handbook*, 2nd ed. New York: Academic, 2001.

[29] U. Ammann, R. Vargas, S. Rees, J. Serra, and J. Roth-Stielow, "An Analytical approach to steady-state current control properties of power converters featuring discrete-time switching," in *Proc. IEEE Power Electronics Specialists Conf., (PESC 2008)*, 2008, pp. 2535–2542.

[30] P. Cortes, J. Rodriguez, D. E. Quevedo, and C. Silva, "Predictive current control strategy with imposed load current spectrum," *IEEE Trans. Power Electron.*, vol. 23, no. 2, pp. 612–618, 2008.

[31] K. Ogata, *Modern Control Engineering*, 3rd ed. Englewood Cliffs, NJ: Prentice Hall, 1996.

[32] V. Blasko, V. Kaura, and W. Niewiadomski, "Sampling of discontinuous voltage and current signals in electrical drives: A system approach," in *IEEE Industry Application Society Annu. Meeting*, 1997, pp. 682–689.